Corrosion behavior of cold rolled and continuously heated SUS 304L stainless steel

Mohammad Javad Sohrabi, Changiz Dehghanian, Hamed Mirzadeh

School of Metallurgy and Materials Engineering, College of Engineering, University of Tehran, Tehran, Iran.

ABSTRACT

The effect of continuous heating after cold deformation on the microstructural evolutions and corrosion behavior of SUS 304L metastable austenitic stainless steel was investigated. After cold rolling with the reduction in thickness of 80%, a microstructure consisting of elongated grains was obtained, in which the X-ray diffraction (XRD) analysis revealed the formation of 96 vol.% strain-induced martensite. The subsequent continuous heating up to 750 °C led to full reversion/recrystallization and the development of an ultrafine grained (UFG) microstructure with an average grain size of 0.45 μm. Continuous heating up to higher temperatures resulted in a significant grain growth, where the average grain size of samples that heated up to 850, 900, 950, and 1100 °C were obtained as 2.5 μm, 5.5 μm, 14 μm, and 45 μm, respectively. The Hall-Patch relationship of $H = 155 + 106/\sqrt{D}$ was developed for the dependence of hardness on the average grain size (D). By grain refinement, corrosion current density (i_{Corr}) increased leading to the worsening of uniform corrosion resistance. However, breakdown potential (E_{Br}) increased by grain refinement, indicating the improved pitting resistance. The Hall-patch-type equations of $i_{Corr} = 0.0147 + 0.4458/\sqrt{D}$ and $E_{Br} = 0.1964 + 0.0695/\sqrt{D}$ were proposed for correlating the corrosion parameters to D.

Keywords: *Stainless steel; Corrosion resistance; Grain refinement; grain growth; Hall-Petch relationship.*

1. Introduction

Nowadays, there is a growing trend toward developing materials with the combination of desirable properties. Among a vast number of alloys, austenitic stainless steels have gained widespread popularity due to their cost-effectiveness as well as good mechanical properties and corrosion resistance [1-3]. Although austenitic stainless steels possess a desirable ductility, they suffer from relatively low strength and hardness [4]. Many efforts have been made to enhance the mechanical strength of stainless steel by benefiting from different strategies. Among them, one of the industrial methods to improve the yield stress of

metallic materials is grain refinement [5-7].

Grain refinement of metallic materials is recognized as a feasible approach for improving both strength and toughness [8]. Due to the absence of phase transitions during heat treatments, other approaches such as recrystallization annealing [9], formation and reversion of strain-induced martensite [10], and severe plastic deformation [11] can be used to refine the grains of austenitic stainless steels. Among them, the formation and reversion of strain-induced martensite to ultrafine-grained (UFG) austenite during elevated temperature annealing by thermomechanical processing is known as a practical method and

highly beneficial for grain refinement that is based on the metastability of the austenite phase [12]. This method has successfully been applied for many austenitic stainless steels [4].
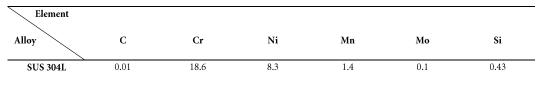
On the other hand, besides mechanical properties, the corrosion behavior of austenitic stainless steels should be considered for the expansion of engineering applications in industry and longer service is the result of higher corrosion resistance performance [13]. The protective layer (mostly chromium oxide) that forms on the alloy's surface is responsible for its remarkable resistance to corrosion, especially uniform corrosion [14]. However, the primary problem with these alloys is the localized pitting corrosion behavior [15,16]. It is worth mentioning that previous works reported the dependency of corrosion resistance on the average grain size and emphasized the significance of grain size on the corrosion resistance of engineering material [17], especially austenitic stainless steels [18-20]. As a result, investigating how grain size affects corrosion resistance is crucial. By grain refinement, grain boundaries obtain greater energy and chemical activity, thus a high density of these boundaries might impact corrosion resistance

[21,22]. On the other hand, grain refinement might lead to a denser and more appropriate passive film, which is important for the pitting corrosion resistance [21].

In this work, the authors aimed to evaluate the effect of grain size on hardness and corrosion performance. In this regard, an SUS 304L stainless steel as the most important stainless steel alloy was considered. By thermomechanical processing including cold rolling and annealing, a wide range of grain sizes was produced and the effect of grain size on mechanical and corrosion properties was examined.

2. Experimental details

The experiments were conducted on a SUS 304L austenitic stainless steel sheet with a thickness of 5 mm and annealed condition. The chemical composition of this alloy is shown in Table 1. The as-received sample was multi-pass rolled to reduce the thickness by 80% (to obtain a thickness of 1 mm) at the nominal temperature of 0 °C (combination of water and ice). Afterward, the cold rolled samples were continuously heated from room temperature up to 1100 °C at the heating rate of 5 °C/min to

Table 1- Chemical composition (wt.%) of the studied alloy

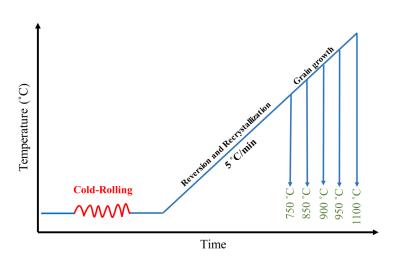| Element / Alloy	C	Cr	Ni	Mn	Mo	Si
SUS 304L	0.01	18.6	8.3	1.4	0.1	0.43

Fig. 1- Schematic representation of the applied processing route in the present work.

obtain equiaxed microstructures with different grain sizes by the occurrence of reversion [23], recrystallization, and grain growth [24,25]. In this regard, during continuous heating, samples were water-quenched at 750, 850, 900, 950, and 1100 °C. For better understanding, the schematic of the process performed in this paper is illustrated in Figure 1.

For microstructural analysis, following standard metallographic sample preparation methods, electrolytic polishing (H_3PO_4-H_2SO_4 solution at 40 V for 40 s [26]) and electroetching (60% HNO_3 solution at 2 V for 20 s) were used to reveal the microstructures. Microstructural investigation on the RD-TD plane [27] of the sheets was performed using a field-emission scanning electron microscope (FEI NOVA NANOSEM 450 FE-SEM). Grain size measurements were based on the standard intercept method (ASTM E112 [28]). Moreover, phase identification was performed by the X-ray diffraction (XRD) technique using a PHILIPS diffractometer with Cu-kα radiation and X'Pert High Score Plus software, where the 2θ angles between 70 and 95°, the step size of 0.02°, and the scan rate of 3°/min were employed. Based on the diffraction peaks, the amount of α′-martensite was

calculated by Equation 1 [29]:

$$f_{\alpha'} = I_{(211)\alpha'} / \{I_{(211)\alpha'} + 0.65(I_{(311)\gamma} + I_{(220)\gamma})\} \quad (1)$$

Mechanical properties were studied by hardness testing, which was performed based on the Vickers hardness using a load of 5 kg and considering an average of five points. The dependency of hardness data on the average grain size (D) was fitted according to the Hall-Petch relationship as follows [30,31]:

$$H = H_0 + K / \sqrt{D} \quad (2)$$

where H_0 is the lattice friction and K is the locking parameter or the Hall-Petch slope.

The corrosion performance was examined by potentiodynamic polarization tests. For corrosion experiments, a standard three-electrode configuration in a 3.5 wt% NaCl aqueous solution (supplying Cl^- chloride ions) at room temperature on a 1 cm × 1 cm surface was employed with a Solartron frequency response analyzer (Model SI 1255). The counter and reference electrodes were a platinum electrode and a saturated calomel electrode (SCE), respectively. The polarization
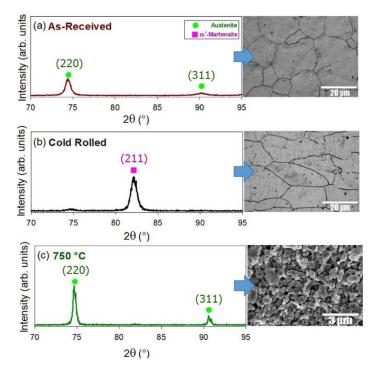

Fig. 2- XRD analysis and corresponding microstructure of (a) as-Received, (b) cold rolled, and (c) cold rolled and continuously heated up to 750 °C samples.

potentials ranged from ~-0.6 to ~0.4 V and the scan rate of polarization tests was 2 mV/s. The samples were prepared by electropolishing (40 V, H3PO4-H2SO4 solution at room temperature [32]), and then, the samples were quickly immersed in the 3.5 wt% NaCl aqueous solution and kept there for 2 h in the absence of any external potential to achieve a steady state potential based on the previous works [33,34] before staring the test. Based on the obtained polarization curves, the corrosion potential (E_{Corr}), corrosion current density (i_{Corr}), and breakdown potential (E_{Br}) were obtained based on ASTM G3-14 Standard [35]. The tests were performed three times to ensure the reproducibility of the results.

3. Results and discussion
3.1. Microstructural and phase analysis

The microstructure of the as-received sample is displayed in Figure 2a, demonstrating a fully equiaxed microstructure with an average grain size of 14 μm. Moreover, the totally austenitic nature of this sample is demonstrated by the XRD patterns of Figure 2a. After 80% cold rolling, the grains became elongated, as shown in Figure 2b. While the

used etching technique does not reveal the phases, the XRD pattern of this sample and Equation 1 reveal that the microstructure is composed of 96 vol.% martensite. It is noteworthy that for microstructural characterization of deformation-induced martensite, the electron backscattered diffraction (EBSD) technique might be used, in which the FCC and BCC phases can be shown in the phase maps [36].

It can be seen that the SUS 304L stainless steel is very susceptible to strain-induced martensite transformation, which is related to the low stability of the austenite phase in this stainless steel, as also shown in previous works [37,38].

As shown in Figure 2c, continuous heating up to 750 °C leads to a fully reversed and recrystallized microstructure with an average grain size of 0.45 μm, which is consistent with the XRD pattern of the sample displayed in Figure 2c. Thus, an UFG microstructure was obtained in this metastable alloy by thermomechanical processing of cold rolling and subsequent annealing, and this led to the significant grain refinement.
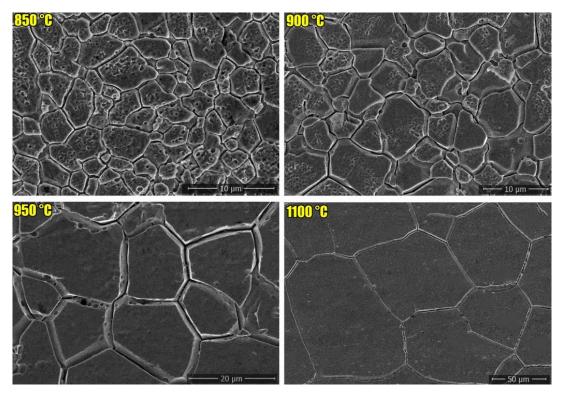
Figure 3 displays the microstructures of

Fig. 3- Representative microstructures of continuously heated samples up to 850, 900, 950, and 1100 °C.

samples that are continuously heated up to higher temperatures. As observed, the significant grain growth compared to that of the reversed/recrystallized sample (Figure 2c) was occurred during heating up to higher temperatures. In this regard, based on the microstructures of Figure 3, the average grain size of samples which heated up to 850, 900, 950, and 1100 °C were 2.5 μm, 5.5 μm, 14 μm, and 45 μm, respectively.

3.2. Evolution of hardness

A wide range of grain sizes from 0.45 to 45 μm was achieved, and afterward, the effect of grain size on hardness as a representative of mechanical behavior was considered. The variations of hardness versus average grain size are shown in Figure 4a. It can be seen that with increasing average grain size, the hardness value continuously decreases. The dependency of hardness on grain size was investigated based on the well-known Hall-Patch relationship (Equation 2), as shown in Figure 4b. As can be seen, the hardness results were in a good correlation with the average grain size according to the Hall-patch relationship of $H = 155 + 106/\sqrt{D}$.

This correlation will be useful for future research works and tailoring the mechanical properties of this alloy.

In this work, effect of grain size on the corrosion behavior is examined for the studied austenitic stainless steel. In this regard, the corrosion current density (i_{Corr}), that is calculated based on the ASTM G3-14 standard, was considered. A higher i_{Corr} is related to a less corrosion resistance for the material [39,40]. On the other hand, pitting corrosion is caused by the local dissolution of passive film and the formation of cavities surrounded by an intact passive surface. The resistance of the passive film against pitting attack can be correlated to breakdown potential (E_{Br}), which is obtained from the polarization curve. The magnitude of E_{Br} is indicative of the pitting resistance [41,42]. As shown in Figure 5, E_{Corr}, i_{Corr} and E_{Br} were obtained based on the polarization curve and the results are also summarized in Figure 5.

As shown in Figure 5, E_{Corr} slightly was shifted toward more noble potential by grain coarsening. Variations of i_{Corr} versus average grain size are shown in Figure 6a. As shown, by grain coarsening,
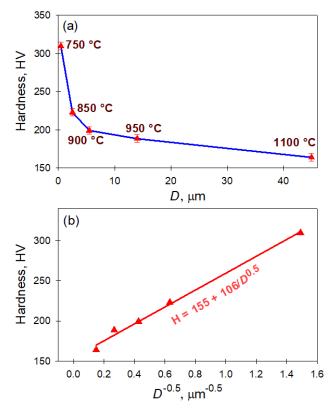

Fig. 4- (a) Hardness vs. grain size and (b) corresponding Hall-Petch plot.

i_{Corr} decreases and the UFG sample with an average grain size of 0.45 µm has the highest uniform corrosion rate. Grain refinement raises the surface's reactivity because it results in higher energies at the grain boundaries and triple junctions, as well as higher electron activity and diffusion rates [21,22].

However, in almost every environment, the protective layer (mostly chromium oxide) forms on the surface of austenitic stainless steel and results in remarkable resistance to uniform corrosion [43].

Consequently, pitting corrosion is also important. In this regard, the evolution of E_{Br} versus average grain size is also shown in Figure 6a. It can be seen that by increasing grain size, E_{Br} decreased and the sample with an average grain size of 45 µm had the lowest E_{Br} and hence the lowest pitting corrosion resistance. In this regard, Sabooni et al. [20] investigated the effect of grain size on the pitting corrosion resistance of AISI 304L stainless steel by using polarization tests and examining the

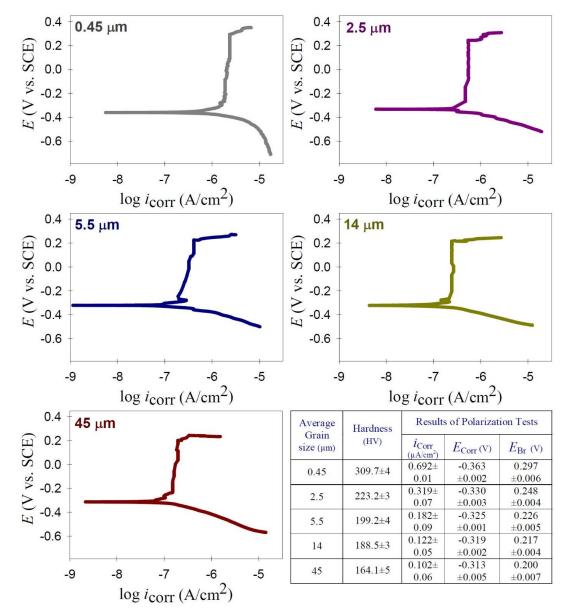| Average Grain size (µm)	Hardness (HV)	Results of Polarization Tests		
		i_{Corr} (µA/cm²)	E_{Corr} (V)	E_{Br} (V)
0.45	309.7±4	0.692±0.01	-0.363±0.002	0.297±0.006
2.5	223.2±3	0.319±0.07	-0.330±0.003	0.248±0.004
5.5	199.2±4	0.182±0.09	-0.325±0.001	0.226±0.005
14	188.5±3	0.122±0.05	-0.319±0.002	0.217±0.004
45	164.1±5	0.102±0.06	-0.313±0.005	0.200±0.007

Fig. 5- Polarization curves of the samples with different grain sizes and summary of corrosion parameters obtained from the polarization curves.

distribution of pits on the surface of the samples. Based on their results, by grain refinement, breakdown potential increased. On the other hand, the diameter and distribution of the pits formed on the surface of samples decreased by grain refinement [20]. Therefore, for passivity behavior, grain refinement will likely result in a more stable protective film and promote pitting corrosion resistance [22].

Further investigation of the relationship between grain size and corrosion parameters for introducing useful equations might be interesting. In this regard, according to Figure 6a and Figure 4a, the dependency of the corrosion parameters on the average grain size is approximately similar to that of the dependency on the hardness values. As a result, it will be interesting to investigate the relationship between corrosion and grain size by the Hall-Patch-type relationships. As shown in Figure 6b, the i_{Corr} results have a good correlation

with the average grain size according to the Hall-patch-type relationship and the dependency of this parameter on the grain size is well established by $i_{Corr} = 0.0147 + 0.4458/\sqrt{D}$. Moreover, the dependency of E_{Br} parameter on the grain size is also explained by $E_{Br} = 0.1964 + 0.0695/\sqrt{D}$, as shown in Figure 6b. As a result, the well-known Hall-Patch-type relationship was used to explain the dependency of corrosion parameters on grain size, and appropriate relationships were presented for the simultaneous improvement of mechanical and corrosion properties in this research work.

5. Conclusions

The corrosion behavior of cold rolled and continuously heated SUS 304L stainless steel with different grain sizes was investigated. The following conclusions can be drawn:

(1) After 80% cold rolling, a microstructure consisting of elongated grains was obtained, in which
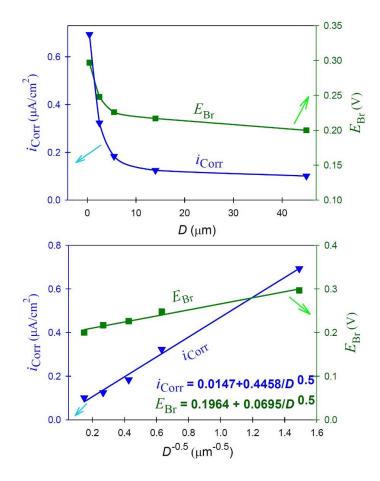

Fig. 6- (a) Dependence of corrosion parameters on the average grain size and (b) corresponding Hall-Petch type relationship.

the XRD analysis revealed the formation of 96 vol.% martensite, indicating the high susceptibility of this alloy to strain-induced martensite transformation. The subsequent continuous heating up to 750 °C led to a fully reversed and recrystallized UFG microstructure with an average grain size of 0.45 μm, representing a remarkable grain refinement when compared to that of the as-received sample with the average grain size of 14 μm.

(2) Continuous heating up to temperatures higher than 750 °C resulted in a significant grain growth compared to that of the reversed/recrystallized sample. In this regard, based on the microstructural analysis, the average grain sizes of samples that heated up to 850 °C, 900 °C, 950 °C, and 1100 °C were obtained as 2.5 μm, 5.5 μm, 14 μm, and 45 μm, respectively.

(3) By increasing average grain size, the hardness value continuously decreased. The dependency of hardness on grain size was investigated based on the well-known Hall-Patch relationship and the relationship of $H = 155 + 106/\sqrt{D}$ was proposed for this material.

(4) By grain coarsening, i_{Corr} decreased and the UFG sample with an average grain size of 0.45 μm showed the highest corrosion rate. However, by increasing grain size, E_{Br} decreased and the sample with an average grain size of 45 μm exhibited the lowest E_{Br} and hence the lowest pitting corrosion resistance.

(5) According to the Hall-patch-type relationship, the equations of $i_{Corr} = 0.0147 + 0.4458/\sqrt{D}$ and $E_{Br} = 0.1964 + 0.0695/\sqrt{D}$ were proposed for correlating the corrosion parameters to the average grain size.

1. Li J, Zhou Z, Wang S, Mao Q, Fang C, Li Y, et al. Deformation mechanisms and enhanced mechanical properties of 304L stainless steel at liquid nitrogen temperature. Materials Science and Engineering: A. 2020;798:140133.

2. Huang M, Wang L, Yuan S, Wang J, Wang C, Mogucheva A, Xu W. Scale-up fabrication of gradient AGS in austenitic stainless steels achieves a simultaneous increase in strength and toughness. Materials Science and Engineering: A. 2022;853:143763.

3. Parnian P, Parsa MH, Mirzadeh H, Jafarian HR. Effect of Drawing Strain on Development of Martensitic Transformation and Mechanical Properties in AISI 304L Stainless Steel Wire. steel research international. 2017;88(8):1600423.

4. Sohrabi MJ, Mirzadeh H, Dehghanian C. Significance of Martensite Reversion and Austenite Stability to the Mechanical Properties and Transformation-Induced Plasticity Effect of Austenitic Stainless Steels. Journal of Materials Engineering and Performance. 2020;29(5):3233-42.

5. Edalati K, Bachmaier A, Beloshenko VA, Beygelzimer Y, Blank VD, Botta WJ, et al. Nanomaterials by severe plastic deformation: review of historical developments and recent advances. Materials Research Letters. 2022;10(4):163-256.

6. Mirzadeh, H., 2023. Superplasticity of fine-grained austenitic stainless steels: A review. Journal of Ultrafine Grained and Nanostructured Materials, 56(1), pp.27-41.

7. Sohrabi MJ, Mirzadeh H, Geranmayeh AR, Mahmudi R. Grain size dependent mechanical properties of CoCrFeMnNi high-entropy alloy investigated by shear punch testing. Journal of Materials Research and Technology. 2023;27:1258-64.

8. Sohrabi MJ, Mirzadeh H, Sadeghpour S, Mahmudi R. Grain size dependent mechanical behavior and TRIP effect in a metastable austenitic stainless steel. International Journal of Plasticity. 2023;160:103502.

9. Geshani MS, Mirzadeh H, Sohrabi MJ. Detailed Hall–Petch Analysis of Cold Rolled and Annealed Duplex 2205 Stainless Steel. steel research international. 2022;93(7).

10. Sunil S, Kapoor R, Singh JB. Reversion of strain induced martensite to achieve high strength and ductility in AISI 304 L. Materials Characterization. 2023;205:113353.

11. Muñoz JA, Chand M, Signorelli JW, Calvo J, Cabrera JM. Strengthening of duplex stainless steel processed by equal channel angular pressing (ECAP). The International Journal of Advanced Manufacturing Technology. 2022;123(7-8):2261-78.

12. Järvenpää A, Jaskari M, Kisko A, Karjalainen P. Processing

and Properties of Reversion-Treated Austenitic Stainless Steels. Metals. 2020;10(2):281.

13. Sedriks AJ. Corrosion of Stainless Steels. Encyclopedia of Materials: Science and Technology: Elsevier; 2001. p. 1707-8.

14. Olsson COA, Landolt D. Passive films on stainless steels—chemistry, structure and growth. Electrochimica Acta. 2003;48(9):1093-104.

15. Xie W, Ding J, Wei X, Wang W, Xia G, Xing J. Corrosion Resistance of Stainless Steel and Pure Metal in Ternary Molten Nitrate for Thermal Energy Storage. Energy Procedia. 2019;158:4897-902.

16. Li J, Mao Q, Chen M, Qin W, Lu X, Liu T, et al. Enhanced pitting resistance through designing a high-strength 316L stainless steel with heterostructure. Journal of Materials Research and Technology. 2021;10:132-7.

17. Savaedi Z, Mirzadeh H, Aghdam RM, Mahmudi R. Effect of grain size on the mechanical properties and bio-corrosion resistance of pure magnesium. Journal of Materials Research and Technology. 2022;19:3100-9.

18. Di Schino, A., Barteri, M. and Kenny, J.M., 2003. Grain size dependence of mechanical, corrosion and tribological properties of high nitrogen stainless steels. Journal of materials science, 38, pp.3257-3262.

19. Hamada AS, Karjalainen LP, Somani MC. Electrochemical corrosion behaviour of a novel submicron-grained austenitic stainless steel in an acidic NaCl solution. Materials Science and Engineering: A. 2006;431(1-2):211-7.

20. Sabooni S, Rashtchi H, Eslami A, Karimzadeh F, Enayati MH, Raeissi K, et al. Dependence of corrosion properties of AISI 304L stainless steel on the austenite grain size. International Journal of Materials Research. 2017;108(7):552-9.

21. Ralston KD, Birbilis N. Effect of Grain Size on Corrosion: A Review. CORROSION. 2010;66(7):075005--13.

22. Ralston KD, Birbilis N, Davies CHJ. Revealing the relationship between grain size and corrosion rate of metals. Scripta Materialia. 2010;63(12):1201-4.

23. Amininejad A, Jamaati R, Hosseinipour SJ. Influence of Deformation and Post-Annealing Treatment on the Microstructure and Mechanical Properties of Austenitic Stainless Steel. Transactions of the Indian Institute of Metals. 2021.

24. Najafkhani F, Kheiri S, Pourbahari B, Mirzadeh H. Recent advances in the kinetics of normal/abnormal grain growth: a review. Archives of Civil and Mechanical Engineering. 2021;21(1).

25. Shirdel M, Mirzadeh H, Parsa MH. Abnormal grain growth in AISI 304L stainless steel. Materials Characterization. 2014;97:11-7.

26. Naghizadeh M, Mirzadeh H. Elucidating the Effect of Alloying Elements on the Behavior of Austenitic Stainless Steels at Elevated Temperatures. Metallurgical and Materials Transactions A. 2016;47(12):5698-703.

27. Mohammadzehi S, Mirzadeh H. Cold unidirectional/cross-rolling of austenitic stainless steels: a review. Archives of Civil and Mechanical Engineering. 2022;22(3).

28. Test Methods for Determining Average Grain Size. ASTM International.

29. Fultz B, Howe JM. Transmission Electron Microscopy and Diffractometry of Materials. Springer Berlin Heidelberg; 2001.

30. Sohrabi MJ, Mirzadeh H, Sadeghpour S, Mahmudi R. Explaining the drop of work-hardening rate and limitation of transformation-induced plasticity effect in metastable stainless steels during tensile deformation. Scripta Materialia. 2023;231:115465.

31. Mehranpour MS, Heydarinia A, Emamy M, Mirzadeh H, Koushki A, Razi R. Enhanced mechanical properties of AZ91 magnesium alloy by inoculation and hot deformation. Materials Science and Engineering: A. 2021;802:140667.

32. Sohrabi MJ, Mirzadeh H, Dehghanian C. Unraveling the effects of surface preparation on the pitting corrosion resistance of austenitic stainless steel. Archives of Civil and Mechanical Engineering. 2020;20(1)

33. Rahman SU, Atta Ogwu A. Corrosion and Mott-Schottky probe of chromium nitride coatings exposed to saline solution for engineering and biomedical applications. Advances in Medical and Surgical Engineering: Elsevier; 2020. p. 239-65.

34. Rahmatian B, Ghasemi HM, Heydarzadeh Sohi M, De Baets P. Tribocorrosion and corrosion behavior of double borided layers formed on Ti-6Al-4V alloy: An approach for applications to bio-implants. Corrosion Science. 2023;210:110824.

35. Practice for Conventions Applicable to Electrochemical Measurements in Corrosion Testing. ASTM International.

36. Sohrabi MJ, Mirzadeh H, Sadeghpour S, Mahmudi R. Dependency of work-hardening behavior of a metastable austenitic stainless steel on the nucleation site of deformation-induced martensite. Materials Science and Engineering: A. 2023;868:144600

37. Zergani A, Mirzadeh H, Mahmudi R. Mechanical response of a metastable austenitic stainless steel under different deformation modes. Materials Science and Technology. 2021;37(1):103-9.

38. Sohrabi MJ, Mirzadeh H, Sadeghpour S, Geranmayeh AR, Mahmudi R. Tailoring the strength-ductility balance of a commercial austenitic stainless steel with combined TWIP and TRIP effects. Archives of Civil and Mechanical Engineering. 2023;23(3).

39. Soleimani, M., Mirzadeh, H. and Dehghanian, C., 2020. Effect of grain size on the corrosion resistance of low carbon steel. Materials Research Express, 7(1), p.016522.

40. Savaedi Z, Mirzadeh H, Aghdam RM, Mahmudi R. Thermal stability, grain growth kinetics, mechanical properties, and bio-corrosion resistance of pure Mg, ZK30, and ZEK300 alloys: A comparative study. Materials Today Communications. 2022;33:104825.

41. Ferreira EA, Silva RCDC, Costa LAT, de Oliveira CPR, Silva GC, Paula AdS, et al. Is duplex stainless steel more corrosion resistant than 316L in aqueous acid chloride-containing environments at temperatures higher than 100°C? Corrosion Engineering, Science and Technology. 2018;53(7):502-9.

42. Pahlavan S, Moayed MH, Mirjalili M. The Contrast between the Pitting Corrosion of 316 SS in NaCl and NaBr Solutions: Part I. Evolution of Metastable Pitting and Stable Pitting. Journal of The Electrochemical Society. 2019;166(2):C65-C75.

43. Shih C-C, Shih C-M, Su Y-Y, Su LHJ, Chang M-S, Lin S-J. Effect of surface oxide properties on corrosion resistance of 316L stainless steel for biomedical applications. Corrosion Science. 2004;46(2):427-41.